Gamma Ray Imager on the DIII-D Tokamak

D.C. Pace,[1,a)] C.M. Cooper,[2] D. Taussig,[1] N.W. Eidietis,[1] E.M. Hollmann,[3] V. Riso,[4] M.A. Van Zeeland,[1] and M. Watkins[1]

[1)] *General Atomics, P.O. Box 85608, San Diego, CA 92186-5608, USA*

[2)] *Oak Ridge Associated Universities, Oak Ridge, TN 37830, USA*

[3)] *University of California-San Diego, 9500 Gilman Dr., La Jolla, CA 92093-0417, USA*

[4)] *State University of New York-Buffalo, 12 Capen Hall, Buffalo, NY 14260-1660*

(Dated: 22 March 2016)

A gamma ray camera is built for the DIII-D tokamak [J. Luxon, *Nucl. Fusion* **42**, 614 (2002)] that provides spatial localization and energy resolution of gamma flux by combining a lead pinhole camera with custom-built detectors and optimized viewing geometry. This diagnostic system is installed on the outer midplane of the tokamak such that its 123 collimated sightlines extend across the tokamak radius while also covering most of the vertical extent of the plasma volume. A set of 30 bismuth germanate detectors can be secured in any of the available sightlines, allowing for customizable coverage in experiments with runaway electrons in the energy range of 1 − 60 MeV. Commissioning of the gamma ray imager includes the quantification of electromagnetic noise sources in the tokamak machine hall and a measurement of the energy spectrum of background gamma radiation. First measurements of gamma rays coming from the plasma provide a suitable testbed for implementing pulse height analysis that provides the energy of detected gamma photons.

[a)] pacedc@fusion.gat.com

I. BACKGROUND

An ultimate requirement for the development of electricity generation from magnetically confined plasmas in a tokamak[1] configuration is that the power plant be capable of surviving off-normal events. This serves as the impetus for understanding (and eventually, predicting and avoiding) the rapid reduction of plasma confinement known as a disruption[2]. One potentially damaging result of a disruption is that a huge electromagnetic load is placed across the device and results in the deformation of its structure. Another potentially damaging result is that all of the previously confined plasma energy is deposited on plasma facing components. Some of the plasma energy can be converted into runaway electrons, a beam of which can reach MA of current with energies in the tens of MeV. The destructive power of a runaway electron beam is of particular concern for ITER[3], which may produce especially potent beams due to its large size[4] and its high plasma current[5].

In order to advance the experimental investigation of runaway electrons, a gamma ray imager (GRI) has been developed at the DIII-D National Fusion Facility[6,7]. The GRI is designed to provide two-dimensional (i.e., across the (R_{major}, z) plane) measurements of the number density and energy of gamma rays produced by runaway electrons following disruptions[8] in the DIII-D tokamak. Gamma rays (traditionally known as "hard x-rays" in this context) are produced as Bremsstrahlung radiation when runaway electrons are deflected by the electric fields from charged particles, neutral particles (for impact factors smaller than the effective electron distance from the nucleus), and the solid materials making up the tokamak's plasma facing components. Diagnostics that measure gamma rays have a long history for applications related to determining nuclear reaction rates[9]. More recent works include the study of runaway electrons and here the gamma ray measurements provide information concerning the full gamma spectrum and can be applicable to ITER[10]. The GRI on DIII-D is intended to provide a companion measurement to the synchrotron imaging[11] system that is capable of measuring a 2D profile (integrated over energy) of synchrotron radiation emitted by runaway electron beams.

The GRI takes advantage a newly available midplane port on DIII-D that provides a tangential view of the entire plasma. The diagnostic system itself can be considered as a pinhole camera built of lead. In this regard, the diagnostic combines the brute-force solution of simply using a sufficient amount of lead to block gamma rays, with the elegant solution of custom built detectors and optimized viewing geometry. The details provided here demonstrate the design and commissioning of the GRI, while dedicated runaway electron experiments will be covered in a future treatment.

II. COMPONENTS AND INSTALLATION

A. Collimation Block

The GRI is designed to provide spatial localization of the measured signal. The mass attenuation coefficient[12] of gamma rays in the $1-60$ MeV range passing through lead is $\mu/\rho \approx 4\times10^{-2}$ cm^2/g, meaning that approximately 10 cm of lead should reduce an incident gamma flux by 98%. The design achieves collimated views of gamma radiation in the plasma volume by requiring that non-collimated gammas pass through 10 cm of lead en route to a detector. This is accomplished by designing a traditional pinhole camera geometry in a computer aided design (CAD) program and then ray tracing to identify the sightlines (for a given individual camera pixel) that pass through a total of less than 10 cm of lead. The resulting lead collimator block is shown in the CAD images of Fig. 1(a-c).

Figure 1(a) shows the rear (i.e., facing away from the plasma), of the GRI collimator block. Many of the 123 individual collimator holes are visible. These represent the pixels of the pinhole camera. Additional lead pieces surrounding these collimator holes serve to attenuate far edge sources of gamma rays. The front end of the GRI is shown in Fig. 1(b), where the pinhole is partially visible. The pinhole is a 1×1 cm square featuring a tapered entrance. An exploded view of the collimator is shown in Fig. 1(c). The spacing of the pixels looks smaller in this panel because of their angled path through the primary lead piece. An open distance of 6.8 cm separates this main piece from the pinhole slab.

The GRI collimator block weighs approximately 190 kg. As such, it must be moved throughout the DIII-D machine hall using an overhead crane. A counter-balanced beam is specially constructed for this task, as shown in Fig. 2(a). The vertical separation between the level of the GRI and the level of the counter weights is necessary in order to move the GRI past an unrelated diagnostic installation. Even if that other hardware were not present, a beam would still be necessary for installation. The collimator block attaches to the beam by way of a secondary support beam that eventually secures the block to the

FIG. 1. Computer models of the lead components for the gamma ray imager. (a) The rear panel view highlights many of the exit channels for the 123 sightlines. (b) The front view shows the entrance pinhole. (c) Assorted dimensions for the lead components are shown with some of the side shielding pieces removed.

DIII-D port. Figure 2(b) is a photograph of the GRI in its final position. The apparent gold coloring is due to the Kapton tape used to wrap each of the individual lead pieces. This Kapton wrapping is required for both safety purposes (all lead surfaces must be insulated from human contact) and physics purposes (reducing the size of the electrically conducting volume in order to reduce error field contributions). The detector plate shown in the Figure is a high-temperature plastic surface with indentations at the locations where individual detectors will reach the collimator block.

FIG. 2. Annotated photographs of the gamma ray imager installation procedure showing (a) the counter weight system used to move the GRI within the DIII-D machine hall, and (b) the final secured position of the GRI inside of the re-entrant midplane port.

B. Viewing Geometry

A large midplane port houses the GRI collimator block. The port interface is re-entrant, which allows the GRI collimation block to be inserted inside of the toroidal field coils while remaining outside of vacuum. Specifically, the pinhole is fixed at a location inside of the coils, while the detectors are located just outside of the coils due to the size of the collimation block. This is shown in the CAD diagram of Fig. 3, which also shows a selected set of sightline volumes. Views from the GRI extend across the entire radial extent of the tokamak with a full diameter of 20 cm for each view at the point of tangency.

Following installation of the collimator block, a spatial calibration is performed. A bright light source is placed outside the vessel behind the collimator block. One sightline remains

FIG. 3. CAD view of the gamma ray imager as installed in DIII-D. The horizontal slice is taken at the midplane of the gamma ray imager view.

open while the others are blocked. This results in a light cone produced by the backlighting of the single sightline. A target surface is manually positioned at multiple locations throughout the inside of the vessel and a coordinate measuring machine (CMM) is used to trace the resulting spot on the target. The outline of the spot is measured in addition to a central point. All of these points are identified manually. After collecting multiple spots, the CMM data is processed to produce a best-fit line representing the sightline. The best-fit line is passed to a ray tracing code that calculates the viewing area throughout the solid angle of the view. A ray tracing code is used for this calculation because the measured spot sizes could be skewed by the CMM operator's personal determination of the edge.

Results from a ray tracing calculation for the central channel are shown in Fig. 4. Figure 4(a) is a histogram of the ray intersection positions at the tangency radius of $R_{\mathrm{major}} = 1.2$ m, where R_{major} is the major radius of the tokamak. The code is run with 625 rays, which is apparent in the resolution of the resulting histogram. Scaling tests show that 625 is sufficient to reach a convergence in the output parameters. A line cut through the center of the histogram is plotted in Fig. 4(b) along with a Gaussian best-fit curve. The full width at half-maximum is 10.6 cm, which is consistent with the CAD expectations (noting that the spot size reported by the CAD calculation represents the extreme edges of the views).

FIG. 4. Modeling of the GRI central sightline. (a) Histogram of the ray density at the tangency radius. The horizontal dashed line represents the line cut taken for panel (b). (b) Horizontal line cut (Model) across the vertical position of 0.23 cm with a best-fit Gaussian profile (dashed trace).

C. Detectors and Electronics

Each pixel of the collimator block requires its own detector. A set of 30 detectors have been purchased and installed for the commissioning phase of the GRI. Following the initial physics experiments, the need for any additional detectors will be reviewed. The detectors are custom built by SCIONIX[13] and feature a bismuth germanate ($Bi_4Ge_3O_{12}$, otherwise known as BGO) scintillator crystal that is cylindrical in shape with a 1 cm diameter and 5 cm length as shown in Fig. 5. BGO scintillators were chosen because of previous work building a scintillator array that identified desirable characteristics for experiments. That system[14] measures global gamma ray emission using 2.5×2.5 cm cylindrical scintillators that are expected to absorb approximately 54% of the incident gamma flux. The GRI, however, needs to measure collimated emission and achieves this using scintillators that are twice as long (along the direction of propagation of the gamma rays) in order to increase the absorption to nearly 88% for gamma rays of energy 10 MeV.

The scintillators are packaged along with a silicon PIN diode that is mated at one end of the cylindrical BGO crystal for optimum light collection. A PIN diode is chosen for this diagnostic system because it successfully operates in the magnetic fields ($\mathcal{O}(1)$ T) produced close to the DIII-D toroidal field coils. The inside of the scintillator's aluminum housing

FIG. 5. Schematic of the gamma ray detectors alongside a photograph. All dimensions are presented in units of millimeters.

is coated with a reflective material that further improves the amount of scintillation light reaching the PIN diode. A preamplifier is directly attached the PIN diode (built by SCIONIX as model SC5152). The preamplifier is a high-gain option providing $9 - 10$ mV/fC of amplification with an 80 ns rise time and 300 μs decay time (experimentally observed closer to 100 μs). The decay time is limited by the BGO crystal itself. This decay time is long enough (given the maximum 10 MHz acquisition rate of the digitizer) to allow the GRI to operate in either a current mode or a counter mode. Current mode operation involves connecting the preamplifier directly to a digitizer and recording the DC-output. This signal is proportional to the power flux of gamma rays. Counter mode records a pulse for each individual gamma ray. These pulses can be further analyzed to determine the energy spectrum of the gamma ray flux.

Initial calibration of the energy sensitivity of the detectors is performed using a 60-Co source acquired from Spectrum Techniques[15]. This 1 μCi source provides gamma rays at energies of 1.17 and 1.33 MeV. Individual detectors were calibrated by placing the source immediately adjacent to the scintillator housing. The observed energy resolution was $\delta E/E \sim 30\%$ and the amplitude response was approximately 6 mV/MeV. A separate calibration is required when all of the detectors are installed on the tokamak because local electronics and cabling transfer the signals tens of meters to a radiation protected annex in which the digtizer is secured. This full calibration of the GRI requires a 1000x more powerful radiation source and the process (an administrative process following radiation safety protocols) of acquiring such a source and implementing procedures for its safe use are underway.

Since there are more available sightlines than there are detectors, a method for changing the installation position of detectors was developed. This method involves securing the detectors in place with an aluminum frame. The frame contains 123 threaded holes that are aligned with each collimated view of the lead block. A detector is placed into a threaded tube that then screws into the aluminum plate. Figure 6 shows the aluminum frame with detectors installed. Figure 6(a) shows the plasma facing side of the frame. Each detector is capped with a hemispherical teflon piece that, combined with the plastic plate shown in Fig. 2(b), guides the detector into position at the immediate edge of the collimation channel cut into the lead block. After securing the detectors, the signal cables are attached as shown in Fig. 6(b).

Signals are transferred from the detectors through the radiation shield walls of the DIII-D machine hall, and then on to a digitizer in a separate room. The digitizer, acquired from D-TACQ Solutions Ltd.[16] as model ACQ216CPCI, is a 16-channel unit with 14-bit resolution that streams to 1 GB of onboard memory. Sampling at 5 MHz is sufficient to resolve individual pulses (sufficient as in being able to acquire a typical pulse with enough data points to perform a pulse fit). At the maximum of 10 MHz sampling, the digitizer allows for 2.9 seconds of data acquisition. That duration is generally longer than necessary since most runaway electron experiments involve a pre-determined timing for the disruption that seeds the runaway beam, and only one second of post-disruption acquisition is required to capture all of the ensuing physics.

III. INITIAL RESULTS

A. Noise from Power Systems

The key to acquiring gamma ray energy spectrum information from the GRI is the ability to resolve individual pulses in the measurements. Even with the advanced detector technology that is readily available, the reduction and removal of noise contributions is a major effort for diagnostics that detect individual particles or photons[17,18]. To this end, initial work

FIG. 6. Photographs of the securing structure for the detectors as they are mated to desired channel sightlines in the collimator block. (a) The detector, or plasma, facing side of the aluminum frame showing the individual detectors. (b) The backside of the aluminum frame showing the cable outputs of the installed detectors.

following the installation of the GRI focused on characterizing signal contributions rising from the background sources in the machine hall. An area of concern is the electromagnetic noise produced from the normal operation of assorted high-power systems in the machine hall. For example, the neutral beam heating system at DIII-D is composed of eight distinct ion sources that produce up to 20 MW of heating and current drive power in the tokamak plasma. Diagnostic calibrations for the charge exchange recombination spectrometry[19] (CER) involve firing the neutral beams into neutral gas. These shots feature full magnetic field and beam power, but no plasma.

Figure 7 plots the average noise pulse amplitude generated by a pulse from different neutral beams. The largest noise amplitude occurs when the detectors are left out in the open areas of the machine hall, i.e., when the detector rests outside of the aluminum frame. Notably, the noise contribution is reduced nearly a factor of two when the detectors are fully installed in the GRI. The surrounding aluminum and lead provides an electromagnetic shielding that reduces the undesirable signal pollution from the magnetic field and neutral beams. The bare cables, i.e., cables left exposed in the machine hall without detectors connected, are only slightly less susceptible to noise than an installed detector. Neutral beam-generated GRI signals on the order of 50 mV correspond to gamma rays within the energy range of interest ($1-60$ MeV). Fortunately, the neutral beams turn on/off in 200 μs, allowing their noise contributions to be avoided through appropriate pre-programmed timing of their use. The beams are never fired post-disruption into a runaway electron beam because the lack of significant plasma density would result in the vast majority of their power directly hitting the walls.

FIG. 7. Noise contributions as a function of the neutral beam that is firing (no data is available from the 150L and 150R beams). The Installed (black squares) trace indicates the actual scenario in which the detectors are fully connected to the collimator block. The Cable Only (red diamonds) trace shows the result when the detector is not connected. The Free (blue circles) trace is acquired with the detectors connected, but not installed in the collimator block.

B. Background Radiation

Nuclear operation of the DIII-D tokamak has been in progress for nearly 30 years. Over that time, a considerable set of changes and upgrades have been enacted, yet the result remains that a number of materials (including those more recently installed) have become activated. During a plasma shot, neutrons produced from deuterium-deuterium reactions dominate the radiation environment. Those neutrons further activate the machine hall with short-lived gamma radiation. This gamma spectrum has been measured to determine the typical, non-runaway, gamma ray background.

The gamma background is measured with a separate set of detectors. These two detectors are known as the mobile gamma unit (MGU) because they can be setup anywhere throughout the facility, including outside of the machine hall, and have their measurements recorded on a fast oscilloscope. These detectors use cylindrical 1×5 cm BGO scintillators just as the GRI detectors, and are manufactured by SCIONIX as model 10B50/0.5-E1-BGO-X. The difference with the MGU detectors is that they are connected to photomultiplier tubes (PMTs, Hamamatsu R647 series[20]). The PMTs are more sensitive than the PIN diodes used in the GRI detectors. PMTs cannot be shielded sufficiently to operate in the large magnetic fields of the GRI installation, however, so the MGU is only used for the background gamma measurement (without magnetic field or a plasma) and in plasma experiments it is run in a separate room away from the machine hall.

The background gamma ray spectrum during a runaway electron experiment is shown in Fig. 8. A series of samples are taken following the completion of a plasma experiment and the beginning of a two week maintenance period during which no plasmas were produced.

FIG. 8. Energy spectrum of gamma rays measured as a function of time following the last plasma shot before an extended break in plasma operations.

C. Pulse Detection Results

Data acquired by the BGO detectors contains pulses from gamma rays, noise unique to each channel, and pickup similar across all channels. The data are routinely subject to a series of signal processing algorithms before being analyzed. An example of two data traces, D_1 and D_2, from detectors installed on DIII-D during normal tokamak operation is shown in Fig. 9(a). The signal from D_1 represents plasma-produced radiation, while D_2 is acquired by a detector that is shielded from the plasma (i.e., it is a blind detector providing background reference). The GRI digitizer begins acquisition 50 ms before plasma breakdown, and that data is used to determine signal offsets that are subtracted before further processing. The signal $D_1 - D_2$ is plotted in Fig. 9(b), which demonstrates the significant reduction in noise from ~ 200 mV of noise down to ~ 20 mV. The data are then processed using the Double-Digital Ramp to Gaussian Shaper (D-DRGS) algorithm[21]. This algorithm further reduces the noise to below 10 mV while maintaining the heights of the pulses. The D-DRGS algorithm correctly measures the height of the peak at $t = 7004.815$ ms which is piled onto the previous pulse. A threshold is defined and any peaks on the D-DRGS trace above this threshold are counted as pulses with their heights and timestamps recorded. Using these techniques, pulse height energy spectrums can be generated during runaway electron experiments.

IV. SUMMARY

A gamma ray imager has been installed and commissioned on the DIII-D tokamak. This new diagnostic system will provide two-dimensional measurements of both the number density and energy spectrum of gamma rays with energies in the range of $1 - 60$ MeV. These measurements will quantify the spatiotemporal dissipation of runaway electron beams subject to rapid injection of high-Z (typically argon or neon) gas or frozen pellets. The observed dissipation in such experiments remains considerably faster than predicted[8]. Initial experience with the gamma ray imager has necessarily focused on accounting for noise and background contributions, with the next runaway electron experiments scheduled for the near future.

FIG. 9. Measured gamma radiation from DIII-D shot 162499. (a) Raw traces from an active (D_1) and a blind (D_2) detector. (b) The net signal, $D_1 - D_2$, is produced by subtracting the blind detector signal from the active signal. Final processing with the D-DRGS algorithm produces a set of individual gamma ray pulses (red trace).

ACKNOWLEDGMENTS

The authors would like to thank Vasily Kiptily, Rita Costa Pereira, and Ana Fernandes for valuable discussions and assistance in implementing the pulse height analysis methods; and Paul Schotanus and his colleagues at SCIONIX for their rapid support throughout the commissioning of the GRI. The GRI was designed and fabricated under General Atomics Internal Research and Development support. Testing of the camera on DIII-D was supported in part by the US Department of Energy, Office of Science, Office of Fusion Energy Sciences, using the DIII-D National Fusion Facility, a DOE Office of Science user facility, under Awards DE-FC02-04ER54698, DE-AC05-06OR23100, and DE-FG02-07ER54912. The participation of V. Riso was supported in part by the U.S. Department of Energy, Office of Science, Office of Workforce Development for Teachers and Scientists (WDTS) under the Science Undergraduate Laboratory Internship (SULI) program. DIII-D data shown in this paper can be obtained by following the links at https://fusion.gat.com/global/D3D_DMP.

REFERENCES

[1]J. Wesson, *Tokamaks*, 4th ed., International Series of Monographs on Physics (Oxford Science Publications, 2011).

[2]A. H. Boozer, Phys. Plasmas **19**, 058101 (2012).

[3]http://www.iter.org/.

[4]V. Izzo, E. Hollmann, A. James, J. Yu, D. Humphreys, L. Lao, P. Parks, P. Sieck, J. Wesley, R. Granetz, G. Olynyk, and D. Whyte, Nucl. Fusion **51**, 063032 (2011).

[5]J. R. Martn-Sols, A. Loarte, and M. Lehnen, Phys. Plasmas **22**, 082503 (2015).

[6]J. Luxon, Nucl. Fusion **42**, 614 (2002).

[7]R. Buttery and the DIII-D Team, Nucl. Fusion **55**, 104017 (2015).

[8]E. Hollmann, M. Austin, J. Boedo, N. Brooks, N. Commaux, N. Eidietis, D. Humphreys, V. Izzo, A. James, T. Jernigan, A. Loarte, J. Martin-Solis, R. Moyer, J. Muñoz-Burgos, P. Parks, D. Rudakov, E. Strait, C. Tsui, M. V. Zeeland, J. Wesley, and J. Yu, Nucl. Fusion **53**, 083004 (2013).

[9]V. G. Kiptily, F. E. Cecil, and S. S. Medley, Plasma Phys. Cont. Fus. **48**, R59 (2006).

[10]A. E. Shevelev, E. M. Khilkevitch, V. G. Kiptily, I. N. Chugunov, D. B. Gin, D. N. Doinikov, V. O. Naidenov, A. E. Litvinov, I. A. Polunovskii, and JET-EFDA Contributors, Nucl. Fusion **53**, 123004 (2013).

[11]J. H. Yu, E. M. Hollmann, N. Commaux, N. W. Eidietis, D. A. Humphreys, A. N. James, T. C. Jernigan, and R. A. Moyer, Phys. Plasmas **20**, 042113 (2013).

[12]NIST Standard Reference Database 8 (XGAM), http://www.nist.gov/pml/data/xcom/index.cfm.

[13]http://scionix.nl/.

[14]A. N. James, E. M. Hollmann, and G. R. Tynan, Rev. Sci. Instrum. **81**, 10 (2010).

[15]http://www.spectrumtechniques.com/disc&laminated_sources.htm.

[16]http://www.d-tacq.com/.

[17]R. C. Pereira, A. M. Fernandes, A. Neto, J. Sousa, C. A. F. Varandas, J. Cardoso, C. M. B. A. Correia, M. Tardocchi, M. Nocente, G. Gorini, V. Kiptily, B. Syme, and M. Jennison, IEEE Trans. Nucl. Sci. **58**, 1531 (2011).

[18]R. V. Perez, W. U. Boeglin, D. S. Darrow, M. Cecconello, I. Klimek, S. Y. Allan, R. J. Akers, D. L. Keeling, K. G. McClements, R. Scannell, M. Turnyanskiy, A. Angulo, P. Avila, O. Leon, C. Lopez, O. M. Jones, N. J. Conway, and C. A. Michael,

Rev. Sci. Instrum. **85**, 11D701 (2014).

[19]K. H. Burrell, P. Gohil, R. J. Groebner, D. H. Kaplan, J. I. Robinson, and W. M. Solomon, Rev. Sci. Instrum. **75**, 3455 (2004).

[20]http://www.hamamatsu.com/us/en/R647.html.

[21]A. Fernandes, R. Pereira, D. Valcrcel, D. Alves, B. Carvalho, J. Sousa, V. Kiptily, C. Correia, and B. Gonalves, Fus. Eng. Des. **89**, 259 (2014).

(a)

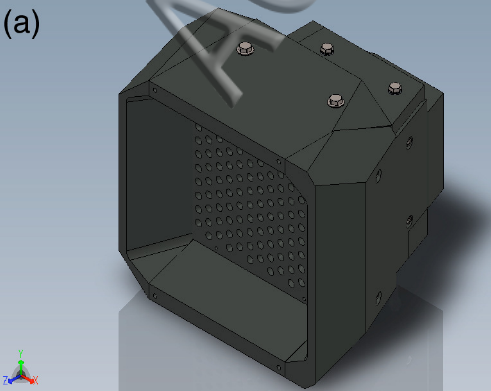

(b)

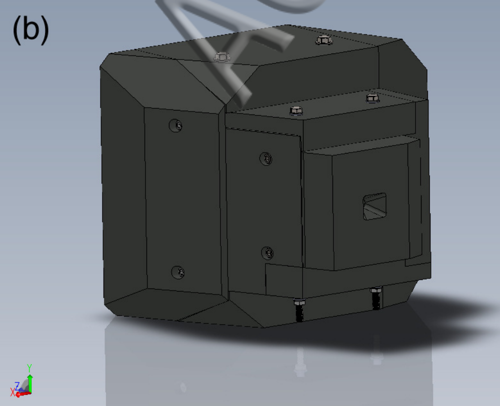

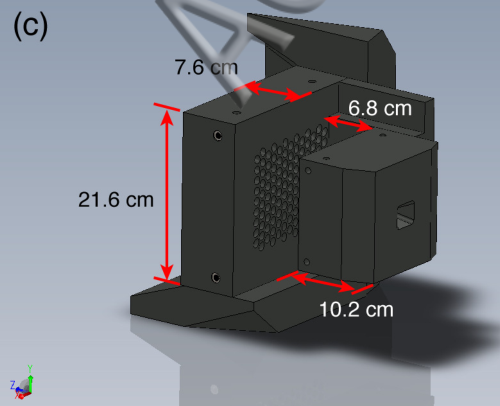
(c)
7.6 cm
6.8 cm
21.6 cm
10.2 cm

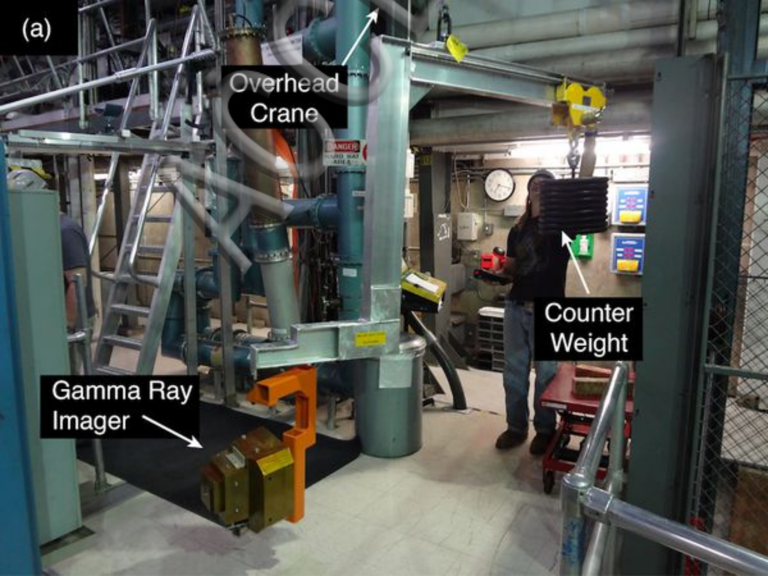
(a)
Overhead Crane
Counter Weight
Gamma Ray Imager

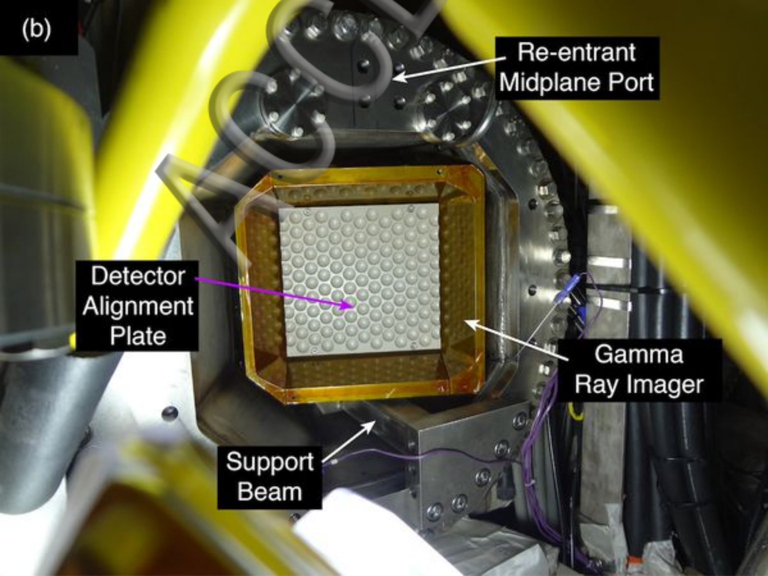
(b)
Re-entrant Midplane Port
Detector Alignment Plate
Gamma Ray Imager
Support Beam

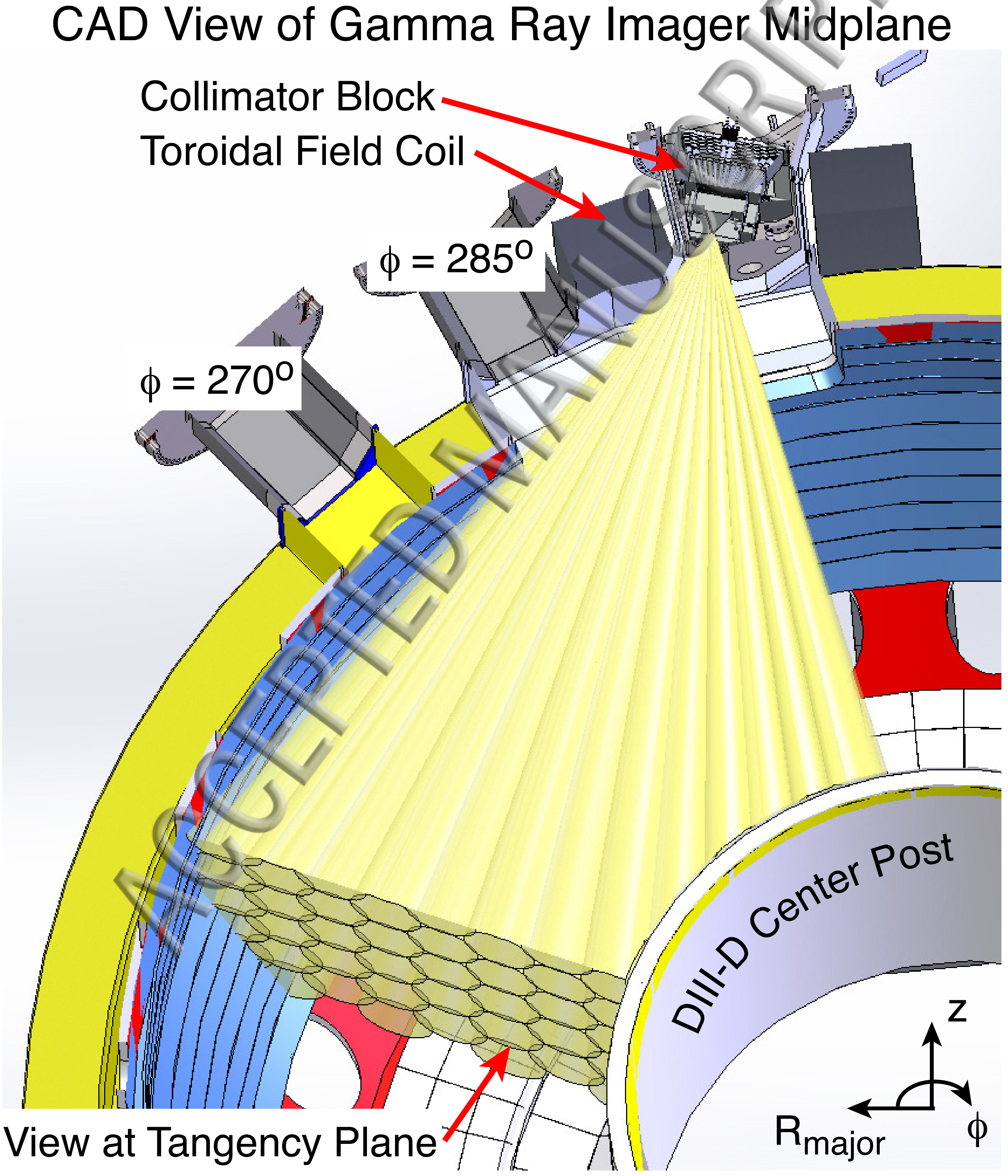
CAD View of Gamma Ray Imager Midplane
Collimator Block
Toroidal Field Coil
ϕ = 285°
ϕ = 270°
DIII-D Center Post
View at Tangency Plane
z
R_{major}
ϕ

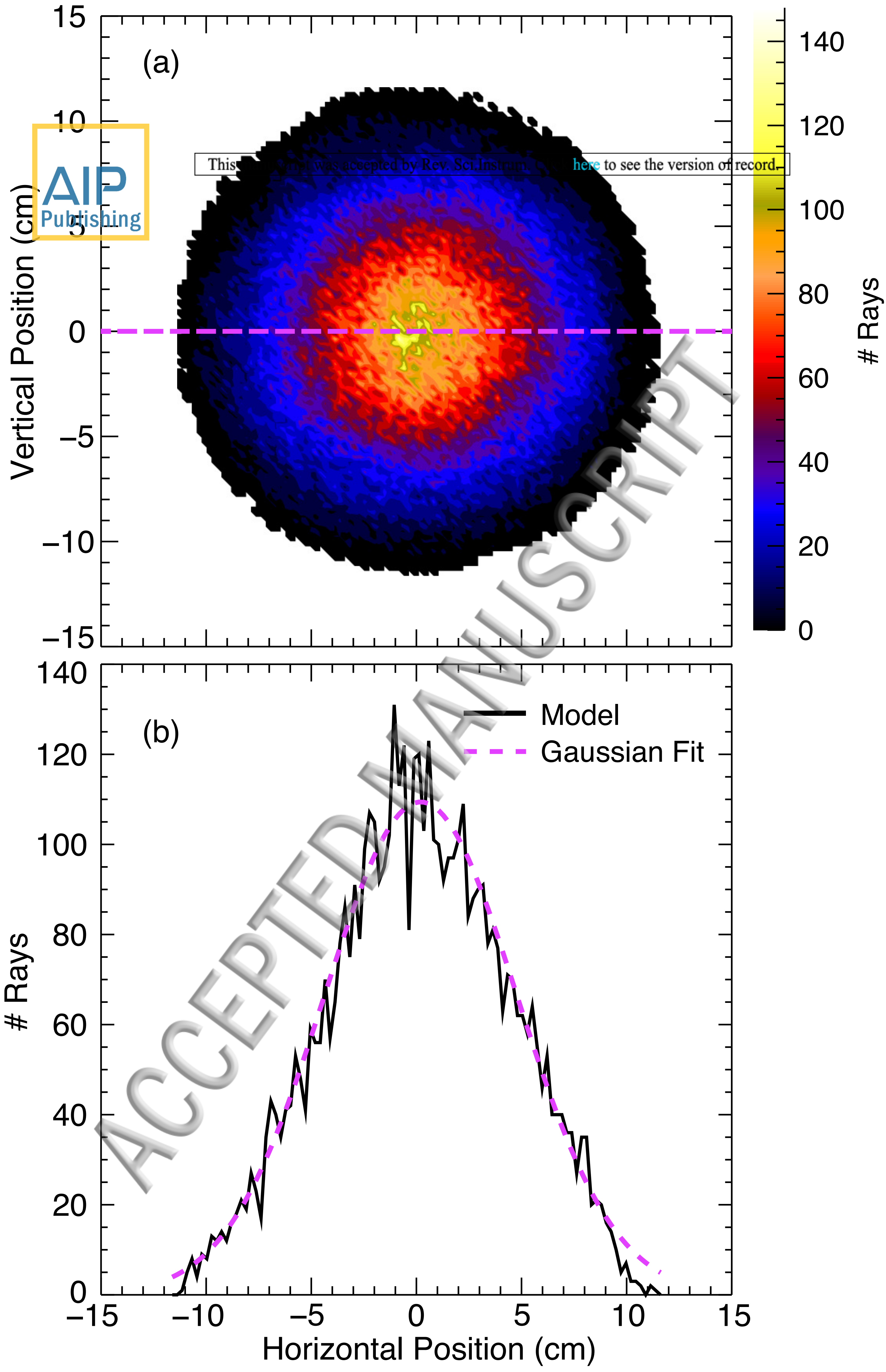
(a)
Vertical Position (cm)
Rays
(b)
Model
Gaussian Fit
Rays
Horizontal Position (cm)

Gamma Ray Detector
(all dimensions in mm)

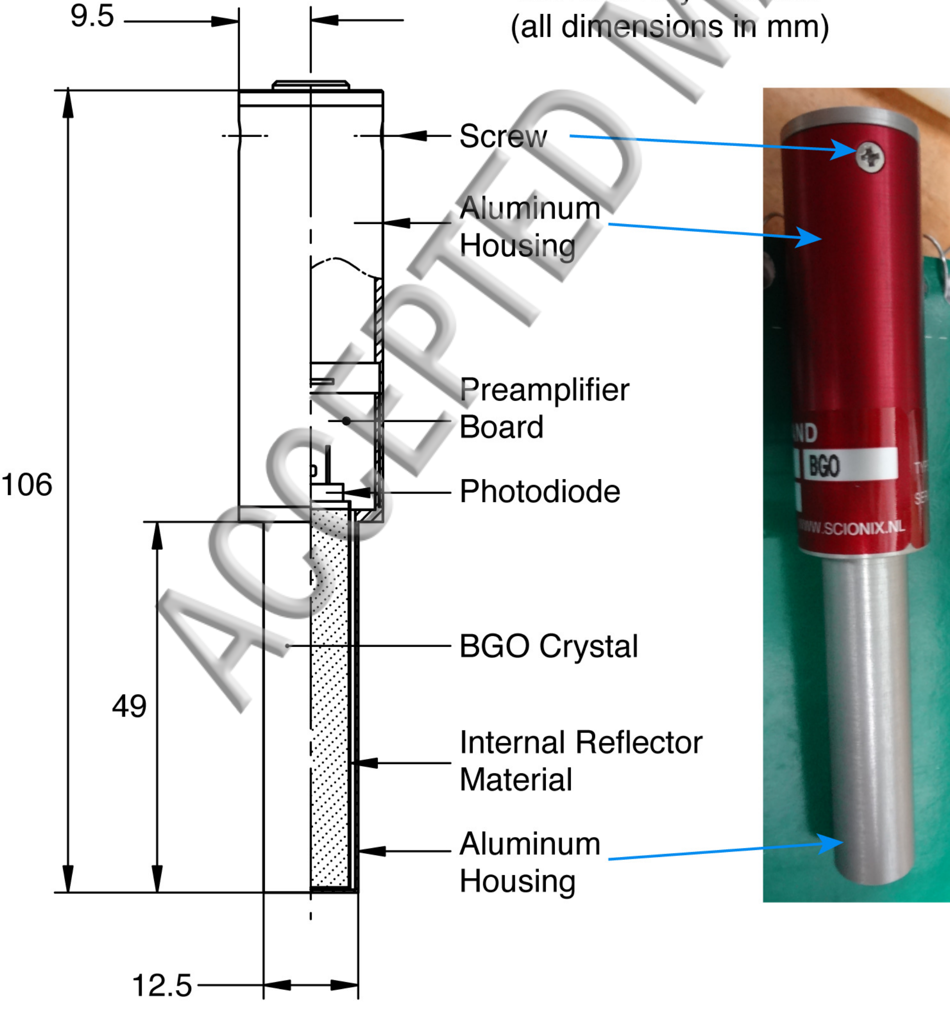

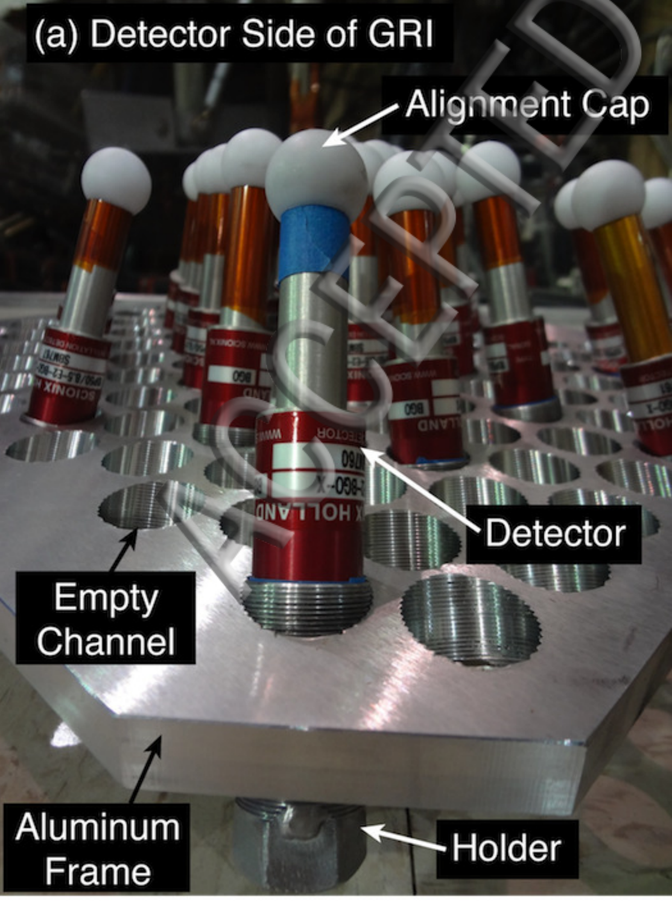
(a) Detector Side of GRI
Alignment Cap
Detector
Empty Channel
Aluminum Frame
Holder

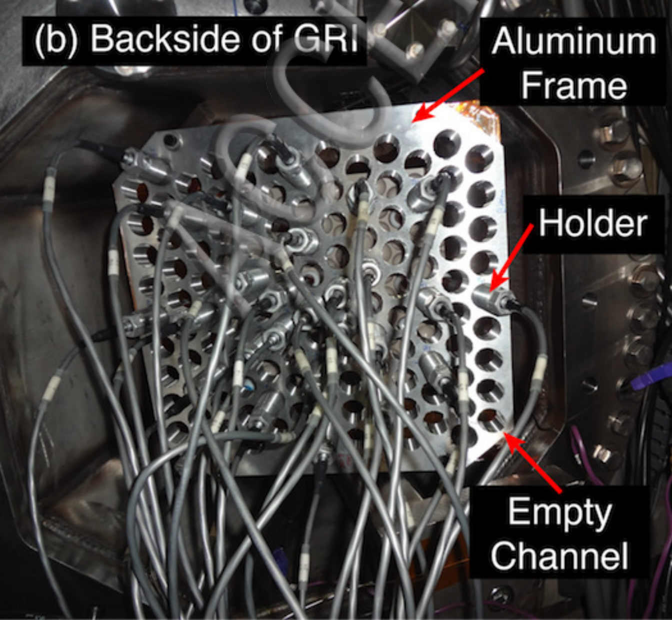
(b) Backside of GRI
Aluminum Frame
Holder
Empty Channel

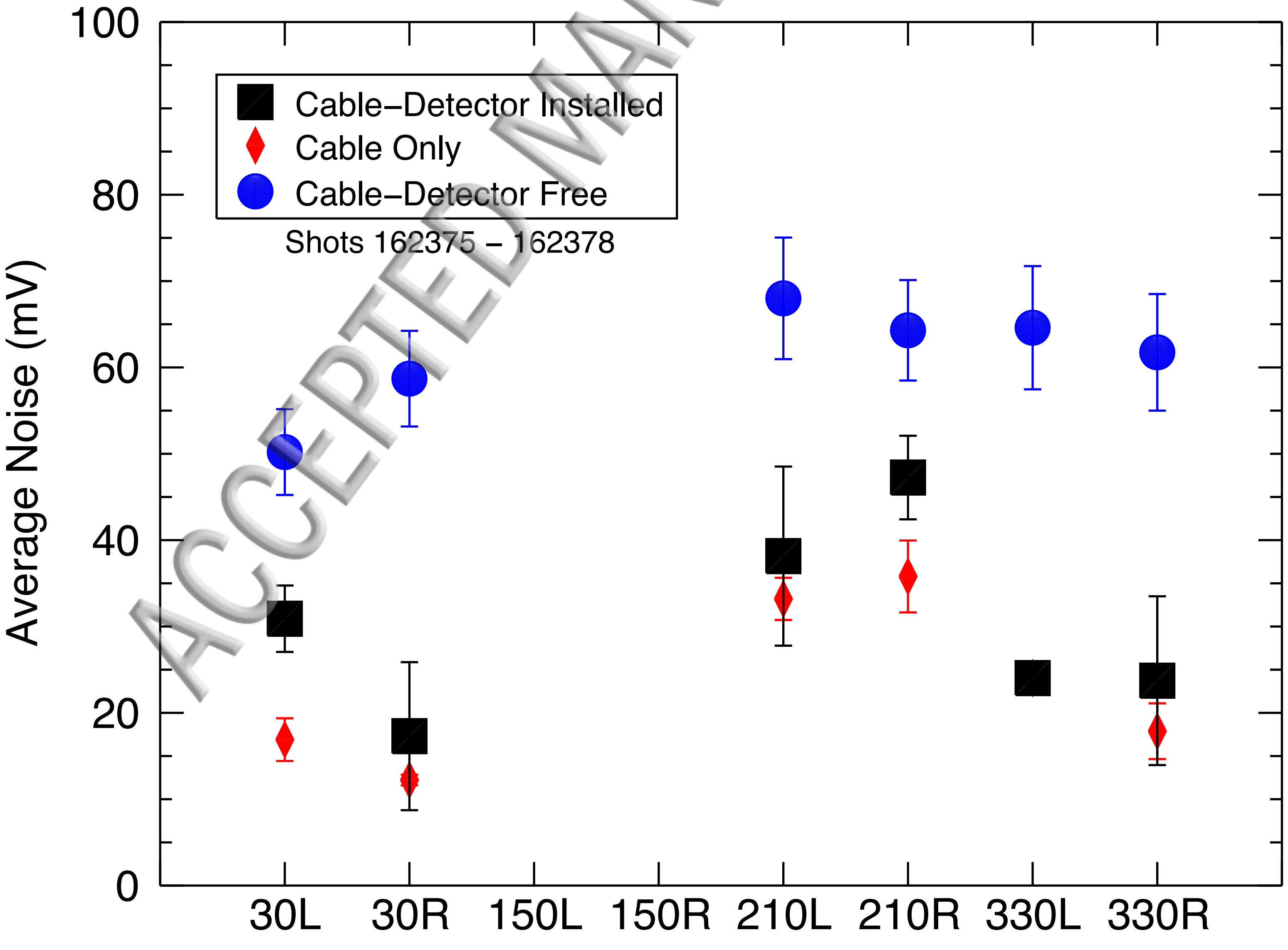

Average Noise (mV)
0
20
40
60
80
100
30L
30R
150L
150R
210L
210R
330L
330R
Cable−Detector Installed
Cable Only
Cable−Detector Free
Shots 162375 – 162378

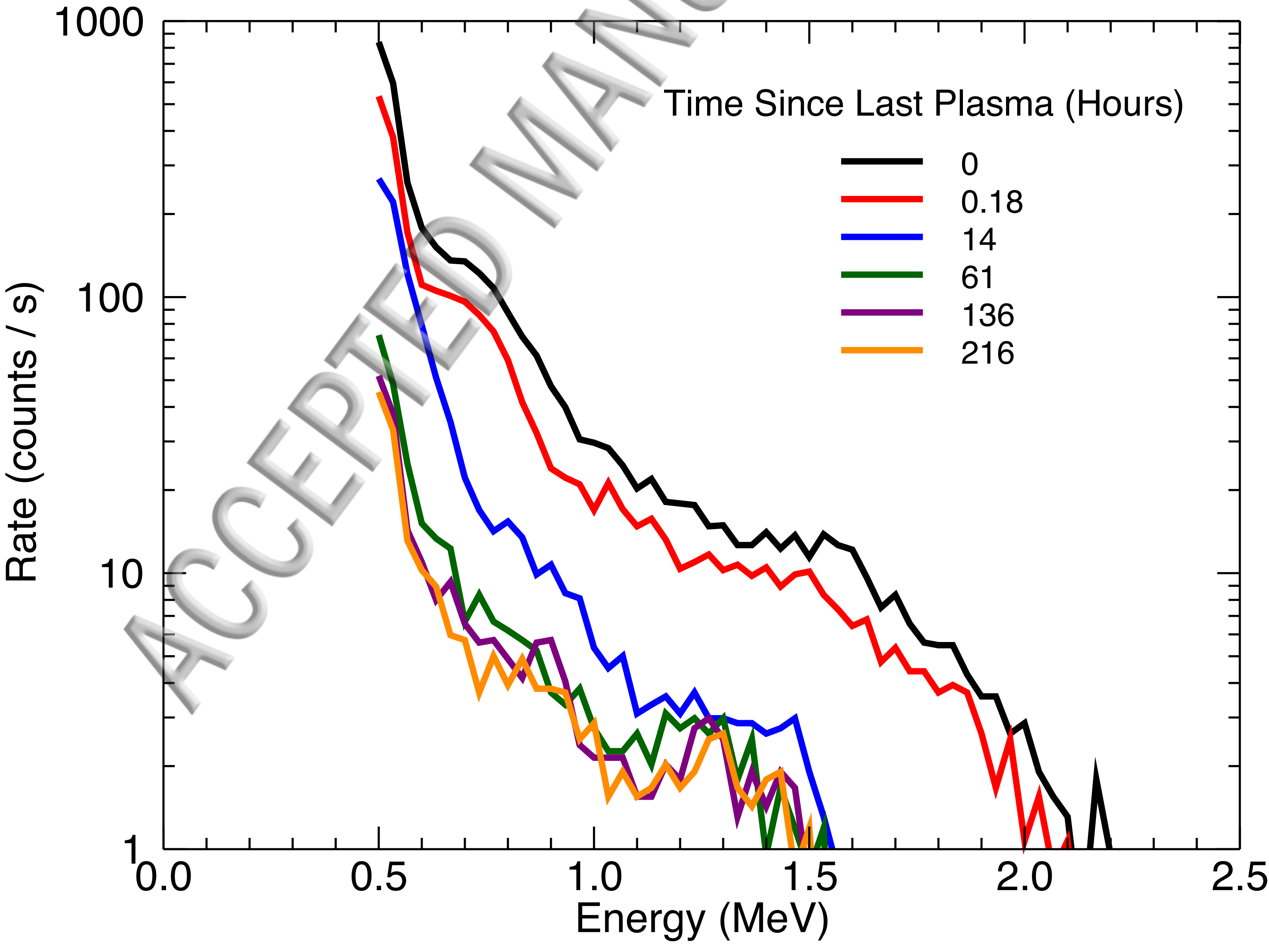

1000
100
10
1
0.0
0.5
1.0
1.5
2.0
2.5
Rate (counts / s)
Energy (MeV)
Time Since Last Plasma (Hours)
0
0.18
14
61
136
216

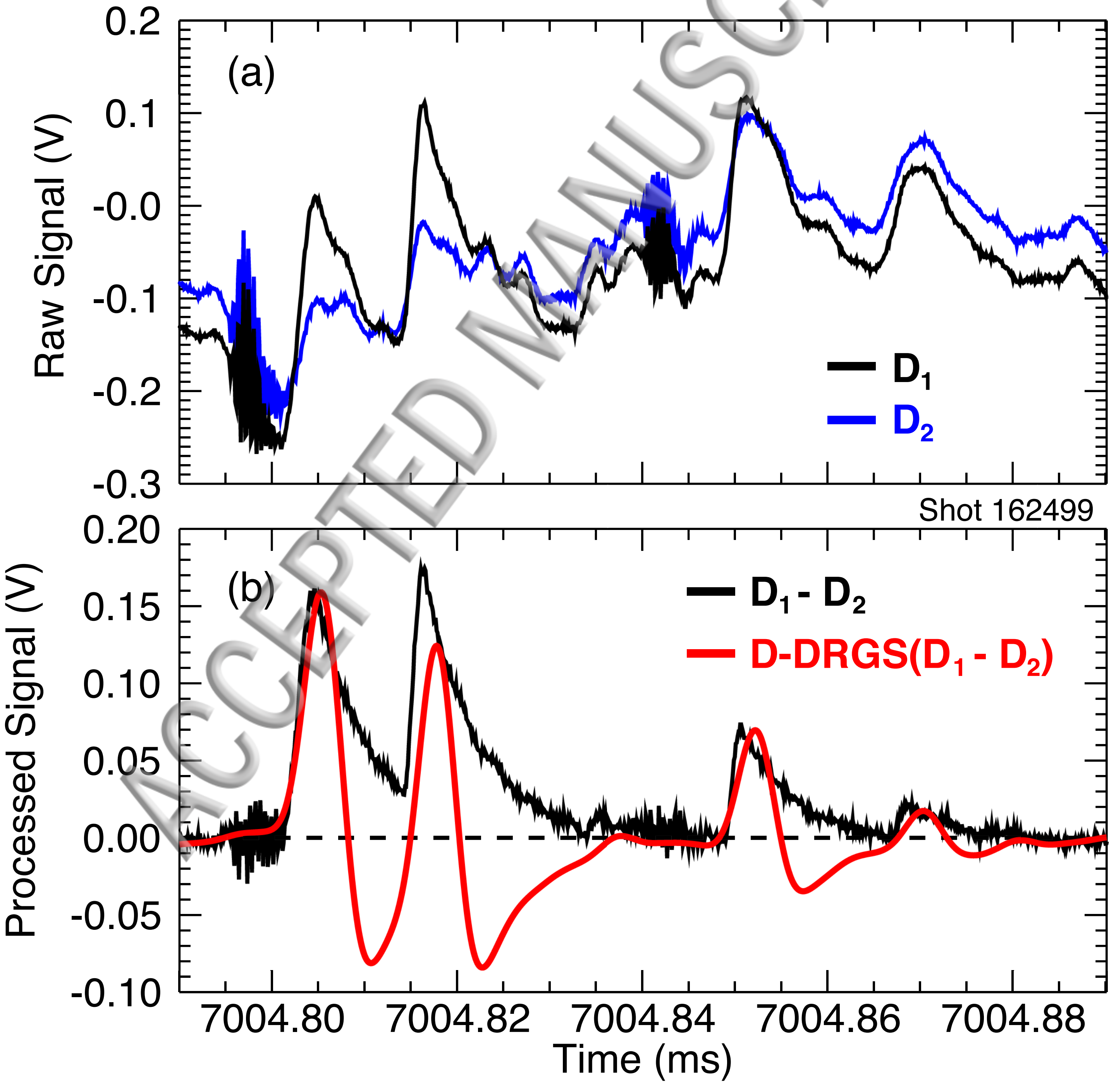

(a)
Raw Signal (V)
0.2
0.1
-0.0
-0.1
-0.2
-0.3
D1
D2
Shot 162499
(b)
Processed Signal (V)
0.20
0.15
0.10
0.05
0.00
-0.05
-0.10
D1 - D2
D-DRGS(D1 - D2)
7004.80
7004.82
7004.84
7004.86
7004.88
Time (ms)